

Article

# A Compact Theory of the Symmetric Compressed-V Dipole Antenna

Ayotunde Ayorinde<sup>1</sup> , Sulaiman Adeniyi Adekola<sup>1,2</sup> , Ike Mowete<sup>1</sup> 

<sup>1</sup>Department of Electrical & Electronics Engineering, University of Lagos, Akoka, Lagos, Nigeria.  
aayorinde@unilag.edu.ng; amowete@unilag.edu.ng .

<sup>2</sup>Department of Electrical & Electronics Engineering, Federal University, Otuoke, Balyesa State, Nigeria  
adekolaadeniyi43@gmail.com

**Abstract**— This paper presents outcomes of a comprehensive investigation of the performance features of the compressed-v-dipole antenna, recently introduced in the literature as being particularly suitable for unmanned surface boat applications. The moment-method solution to the rigorously formulated electric field integral equations for the problem, provided an approximation to the distribution of current on the antenna. A comparison of computational results due to this formulation with available measurement data demonstrated very good agreement between the two; to lend credence to the validity of the formulation. Profiles of the antenna's input and radiation-zone characteristics (including input impedance, return loss, E-field patterns, and maximum directivity) presented in the paper describe how choice of apex angle, antenna electrical length, and degree of compression, influence the performance of the antenna.

**Index Terms**— Compressed V dipole, Pattern reconfigurability, Return loss, Unmanned surface boat

## I. INTRODUCTION

According to several literature sources [1] – [4], one of the key attractions for the V dipole antenna (VDA) derived from a need to resolve an application difficulty associated with the conventional linear dipole antenna. For as noted by these sources, when the linear dipole antenna's electrical length exceeds one wavelength at the operating frequency, its directivity, in the direction normal to the antenna, begins to diminish, mainly because minor lobes of increasingly significant sizes begin to develop. By reshaping the otherwise straight dipole to form a V-shaped structure, minor lobe sizes are drastically reduced, and directivity in the 'normal' direction increases significantly more than that due to the corresponding linear dipole, [1], [2].

Early formal investigations into the V-dipole's performance features are typified by that reported in [5], which, through experimental evidence, established that the VDA with a total arm length of a half wavelength at the operating frequency, provided a radiation pattern that is substantially omnidirectional in the horizontal plane. The particular case of the VDA, whose arms were inclined at 90° to each other

(and referred to as the ‘quadrant antenna’) and excited in anti-phase at the apex, was considered by the paper. A theory of V antennas described in [6], is arguably a leading candidate for the pioneering analytical work on this class of dipole antennas. Through the use of the method of successive approximations, the paper solved an integral equation for the current distribution along the arms of an apex-driven, symmetrical V-antenna, to characterize the antenna’s input impedance. A similar integral equation formulation approach was adopted in [7], for a ‘rectangular’ VDA, through which a variational formula for the input impedance of the ‘quadrant’ antenna considered in the paper, emerged as a second order solution. Another notable analytical contribution presented in [2] treated the VDA as a special case of the general analysis problem for curvilinear thin-wire antennas. In that contribution, the Lorentz gauge was invoked in addition to the boundary condition utilized in [6], such that the integral equation developed for the distribution of current along the antenna’s arms, was characterized by a first order quasi-singularity only.

Further insights into the performance characteristics of the VDA became available with advent of large scale computing facilities, through which, for example, a Method of Moments (MoM) analysis that utilized piecewise sinusoidal basis and testing functions [8] facilitated the investigation of the features of a system of V-antennas mounted on the ATS-E radio astronomy experiment’s satellite system. Similar investigations were reported in [1] and [9], to provide numerical data characterizing current distribution, input impedance, radiation-zone fields, radiation resistance, and directivity / gain profiles for the typical VDA. Results in [1], in addition, prescribed apex angle for optimum directivity, for a given VDA arms’ length; whereas those in [9] suggested that when apex angle is less than  $90^\circ$ , the VDA’s radiation pattern is substantially omnidirectional over a wide bandwidth (at the expense of impedance bandwidth), and that for values of apex angle between  $75^\circ$  and  $80^\circ$ , the lowest resonant length is at least, a quarter wavelength, increasing (for a given wire radius) as arms’ length increases. A related contribution reported in [10] combined the bacteria foraging algorithm (BFA) with the MoM to determine the optimum VDA apex angle, as nominated by corresponding antenna directivity values.

In terms of practical applications, it is readily arguable that the ‘resistively loaded’ VDA (RLVDA) in various configurations, represents the most popular. Preliminary results concerning the antenna characteristics of the RLVDA were presented in [11], where it was described as a ‘travelling wave V-antenna’, configured as two resistively-loaded straight wires, arranged in a V shape, and fed at the apex. Analytical [12] and experimental [11] results presented suggest that the antenna performs best when the loading resistance is located a quarter wavelength away from the antenna’s end, and that its characteristic radiation pattern profiles indicate that it is particularly suitable for space observation applications. At about the same period, two other investigations, [13], [14] focused on the travelling wave V antenna, in this case, conceptualized as a combination of a travelling wave dipole antenna and a resonant V antenna. By locating a set of terminating resistors close to the end of the antenna arms, it

was ensured, through a proper choice of loading resistance, that between the feed point and the terminating resistors, current substantially distributes as a travelling wave. Results presented in the publications comprehensively described the influence on radiation patterns, of load resistance, apex angle, and extent of the traveling wave and standing wave segments of antenna arm length. One attribute of the RLVDA identified in [14] is that of its radiation pattern being of the 'pencil-beam' type, over a wide frequency band. It is noted in [15] that this attribute is a key requisite in ground penetrating radar (GPR) applications, which require a broadband antenna able to radiate a short pulse directed at a small spot on the ground. As pointed out in [15], although the resistively loaded dipole antenna (of the type described for example in [16]) meets the wideband requirement, it is, unlike the RLVDA, lacking in the desired directivity. And whereas RLVDA is able to provide a highly directive, broadband radiation, its impedance matching ability is such that it is characterized by a rather high voltage standing wave ratio (VSWR) at the input, [17]. In order to improve the VSWR (as well as gain and front-to-back ratio) therefore, the contribution in [17] introduced geometrical and distributed loading profile modifications to the RLVDA of [15]. The geometrical modification produced a V- dipole antenna, whose arms are smoothly curved from its feed lines, and for which the distributed loading profile is defined [17, (4)] by a modification of (1) of [15].

A few other variants of the conventional VDA have also been introduced in the literature, to address different practical application needs. These include the double V dipole antenna, whose conventional form [18], [19] includes two coplanar VDAs sharing a common feeding arrangement. Analytical and experimental results presented in the publications demonstrated that the 'double-vee' dipole antenna is more highly directive and has lower sidelobe levels than the conventional VDA, and can consequently be utilized to advantage, with applications of the latter. A variation of this configuration was presented in [20], in which the two VDAs remained coplanar, but with only one of them excited, and the arms of the other acting as reflectors, to produce an antenna suitable for ultra-wideband (UWB) applications. The Double-Double-Vee antenna analyzed in [21] is said to be particularly suitable for satellite image acquisition applications. An interesting variant of the VDA, in which the linear arms are replaced by a series of resistively connected thin-wire ellipses, was presented in [22]. Referred to as the elliptical resistively loaded V dipole (ERLVD) antenna, the device is shown to be suitable for UWB applications, including those that require wideband pulse radiation. For use with near-field optics applications, results presented in [23] for quadrupolar excited V-shaped optical resonant antenna suggest that it is particularly suitable, on account of its strong electric field-enhancing properties. Certain configurations of V dipole antenna systems have also been shown to be particularly suitable for radiation pattern reconfiguration applications. Notable examples include the system presented in [24], which consists of four identical VDAs arranged symmetrically around a centrally located switching circuitry, and whose radiation pattern is controlled by switching to select any combination of the VDAs as may be desired,

for excitation. The system is recommended by the authors, for WLAN applications. Another is the graphene-based VDA proposed in [25] for the radiation of two possible patterns: namely, ‘quasi-isotropic’ and ‘directional’ patterns. The antenna may be described as an array consisting of a VDA and two parasitic elements, (one in the front, and the other, at back of the VDA) and backed by a substrate of SiO<sub>2</sub>. When the directional pattern is desired, the chemical potential of the substrate is modified appropriately; and for the radiation of the quasi-isotropic pattern, the parameters of the VDA are so chosen, as to ensure that pattern nulls in the lateral direction are reduced as much as possible.

Of particular interest to this paper is the ‘compressed V dipole antenna’ (CVDA) introduced, in a recent preprint that appeared online, [26], as being suitable for surface unmanned boat applications. The authors identified their motivation for the investigations as the problem of the ‘blind spots’ that develop for whip antennas routinely mounted on such boats, when the hull is tilted. Because as remarked by the authors, the problem of the CVDA has, as far as can be ascertained, not been treated by any publication, [26], which remains an unpublished manuscript, represents its first treatment in the literature. Without prejudice to the manuscript’s publication status, its key proposals and associated contributions may be identified as follows. First, the manuscript’s theoretical treatment on one hand, conceives the CVDA as an array of three elements, including a VDA and two parasitic elements; and on another hand, as a single element a VDA, to whose tips, horizontal dipoles are connected. And using the latter structure as model, formulates integral equations for the antenna’s far-zone field as a superposition of three fields; each in turn, deriving from the field expression for infinitesimal dipole. Although this analytical treatment was not validated in the manuscript, FEKO-based simulation as well as experimental results concerning the antenna’s radiation-zone field profile were presented in support of the manuscript’s main conclusion, that the CVDA resolves the whip antenna’s ‘blind spot’ problem in surface unmanned boat applications.

It is this paper’s main objective therefore, to present an analytical treatment of CDVA towards characterizing its input and far-zone performance features. And to that end, the paper develops a rigorous formulation of integral expressions for the far-zone fields of the CVDA: which is treated in this paper, as a ‘bent thin-wire V-shaped antenna’, sharply bent at the top of its arms. The distributions of current along the arms of the antenna, the only unknown in the integral expressions, is determined by the method of moments using piecewise linear expansion and testing functions. For the purposes of model validation, the special case of the CVDA, for which ‘compression’ is zero (that is the conventional VDA) is considered: the very good agreement between the results due to this paper’s formulation and published corresponding measurement data ([3],[27]), supported the validity of the formulation. Computational results obtained and presented in graphical formats include those for the CVDA’s input characteristics (current distribution, input impedance, and return loss) as well as radiation-zone parameters of field pattern profiles and directivity. These results reveal that in general,

the CVDA's performance parameters are very sensitive to changes in apex angle, antenna arm's length, and degree of compression; and that its far-zone pattern can be readily re-configured through informed choices of these physical attributes.

The paper, in section II, presents details of the analytical considerations concerning the formulation of the integral expressions for the radiation-zone fields of the CVDA. Computational results for the CVDA's performance parameters are presented and discussed in Section III, while the main findings and associated conclusions of the investigations are highlighted Section IV, which is the concluding section of the paper.

## II. ANALYSIS

Fig. 1a depicts the problem geometry for the CVDA symmetrically located about the z-axis on the y-z plane; with two arms, each consisting of a slant segment (of length denoted by  $L_1$ ) and a horizontal section of length denoted by  $L_2$ .

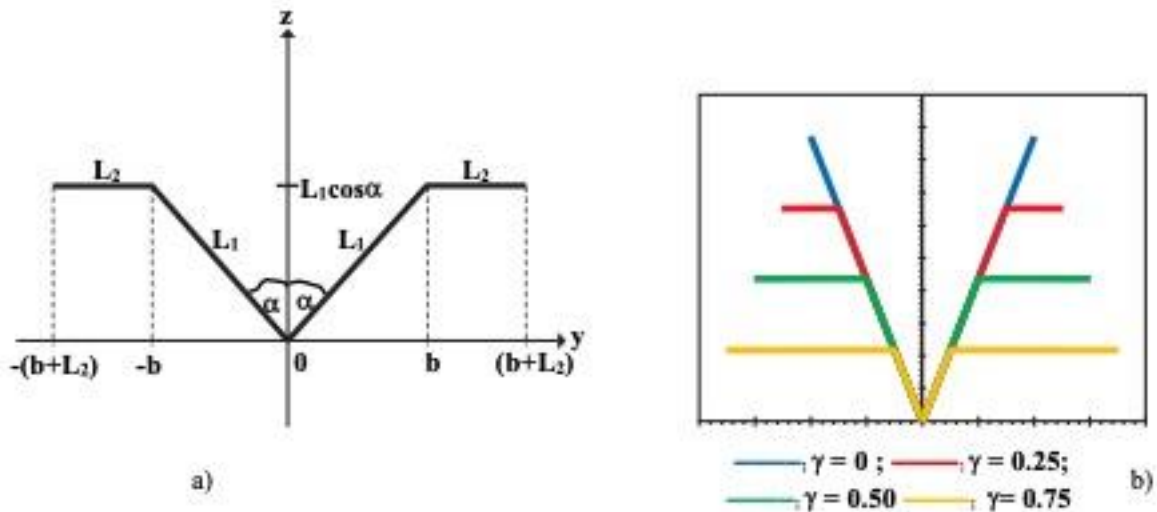


Fig. 1. a) Geometry of a compressed V dipole antenna on the Y-Z plane. b) Illustration of degrees of compression  
 If the symbol  $\gamma$  defines a 'compression factor' such that

$$\begin{aligned} L_1 &= (1 - \gamma)L, \\ L_2 &= \gamma L, \quad 0 \leq \gamma \leq 1 \end{aligned} \quad (1)$$

where  $L = L_1 + L_2$  represents the 'total length' for each arm, then it is easy to see that when  $\gamma$  equals zero, the CVDA transforms to a VDA; and when  $\gamma$  is set to unity, it reduces to a centre-fed linear dipole antenna lying on the horizontal axis. Values of  $\gamma$  in between these two extremes define different degrees of 'compression' in the manner described by Fig. 1b. Using the foregoing notations and definitions, the geometry of the CVDA admits analytical description as follows: for the antenna's right-hand side member (henceforth referred to as 'right arm'),

$$L_R(\alpha, y) = \frac{L_1 \cos \alpha}{b} y [u(y) - u(y-b)] + L_1 \cos \alpha [u(y-b) - u(y-b-L_2)], \quad (2a)$$

and for the ‘left arm’,

$$L_L(\alpha, y) = \frac{L_1 \cos \alpha}{b} y [u(-y) - u(-y-b)] + L_1 \cos \alpha [u(-y-b) - u(-y-b-L_2)]. \quad (2b)$$

In 2(a) and 2(b), ‘ $\alpha$ ’ is the angle between each CVDA slant arm and the z-axis, ‘b’, the y-coordinate of the point at which antenna slant and horizontal arms connect, and  $u(\bullet)$  is the unit step function of its argument. Using these two equations, position vectors may now be defined in terms of  $L_1$  and  $L_2$  and as functions of the ‘compression factor’ symbolized by  $\gamma$ , in the following manner:

$$\vec{r}'_{s1} = \ell' \sin \alpha \hat{a}_y + \ell' \cos \alpha \hat{a}_z, \quad 0 \leq \ell' \leq L_1 \quad (3a)$$

and

$$\vec{r}'_{h1} = y' \hat{a}_y + L_1 \cos \alpha \hat{a}_z, \quad b \leq y' \leq b + L_2, \quad (3b)$$

for the right arm; whilst for the left arm,

$$\vec{r}'_{s2} = -\ell' \sin \alpha \hat{a}_y + \ell' \cos \alpha \hat{a}_z, \quad 0 \leq \ell' \leq L_1 \quad (3c)$$

and

$$\vec{r}'_{h2} = -y' \hat{a}_y + L_1 \cos \alpha \hat{a}_z, \quad -b \leq -y' \leq -(b + L_2). \quad (3d)$$

The subscripts ‘s’ and ‘h’ appearing in (3a) to (3d) identify the slant and horizontal segments of the CVDA, respectively. Unit vectors appropriate to the slant and horizontal segments of the antenna then become available through the use of the well-known definition

$$\hat{a} = \frac{d\vec{r}'}{d\ell'} / \left| \frac{d\vec{r}'}{d\ell'} \right| \quad (4)$$

As

$$\hat{a}_{s1} = \sin \alpha \hat{a}_y + \cos \alpha \hat{a}_z, \quad (5a)$$

and

$$\hat{a}_{h1} = \hat{a}_y; \quad (5b)$$

for the right arm, with corresponding expressions for the left arm emerging as

$$\hat{a}_{s2} = -\sin \alpha \hat{a}_y + \cos \alpha \hat{a}_z, \quad (5c)$$

and

$$\hat{a}_{h2} = -\hat{a}_y \quad (5d)$$

Because it is apparent from the foregoing derivations that there is a one-to-one correspondence between expressions for the symmetrical arms of the CVDA, the ensuing development of the electric field integral equations focuses on the antenna’s right arm: corresponding expressions for the left arm, as is readily verified, directly follow through the simple expedient of substituting  $-\alpha$  for  $\alpha$ , and  $-y$  for  $y$ .

The vector magnetic potential for the problem derives from the well-known expression given as

$$\bar{A} = \frac{\mu_0}{4\pi} \int_{\ell'} \hat{a}_{\ell'} I(\ell') \frac{e^{-j\beta_0 |\bar{r} - \bar{r}'|}}{|\bar{r} - \bar{r}'|} d\ell' \quad (6)$$

in which  $\mu_0$  represents free-space permeability,  $\beta_0$  free-space propagation constant,  $d\ell'$  differential element along wire axis,  $\bar{r}'$  the position vector from the coordinate system origin to a point on the antenna, and  $\bar{r}$  the radial vector from the origin to a far-zone (measurement) point. Invoking the usual far-zone 'magnitude' and 'phase' approximations for the right-hand slant section of the CVDA leads to

$$|\bar{r} - \bar{r}'| = r \quad (7a)$$

in the magnitude term, and

$$|\bar{r} - \bar{r}'| = r - \hat{a}_r \cdot \bar{r}' = r - \ell' \sin\alpha \sin\varphi \sin\theta - \ell' \cos\alpha \cos\theta \quad (7b)$$

in the phase term; with  $\hat{a}_r = \cos\varphi \sin\theta \hat{a}_x + \sin\varphi \sin\theta \hat{a}_y + \cos\theta \hat{a}_z$  and (3a) having been utilized in (7b).

Equation (7b) applies only in the case of the slant segment of the CVDA's right arm. The corresponding expression for the arm's horizontal segment is

$$|\bar{r} - \bar{r}'| = r - \hat{a}_r \cdot \bar{r}' = r - y' \sin\varphi \sin\theta - L_1 \cos\alpha \cos\theta \quad (7c)$$

The use of (5a) and (7) in (6) then yields

$$\bar{A} = \frac{\mu_0 e^{-j\beta_0 r}}{4\pi r} \int_0^{L_1} (\sin\alpha \hat{a}_y + \cos\alpha \hat{a}_z) I(\ell') e^{j\beta_0 \ell' [\sin\alpha \sin\varphi \sin\theta + \cos\alpha \cos\theta]} d\ell' \quad (8)$$

for the arm's slant segment. Clearly, the Cartesian components of this vector potential are

$$A_y = \frac{\mu_0 e^{-j\beta_0 r}}{4\pi r} \int_0^{L_1} \sin\alpha I(\ell') e^{j\beta_0 \ell' [\sin\alpha \sin\varphi \sin\theta + \cos\alpha \cos\theta]} d\ell', \quad (9a)$$

and

$$A_z = \frac{\mu_0 e^{-j\beta_0 r}}{4\pi r} \int_0^{L_1} \cos\alpha I(\ell') e^{j\beta_0 \ell' [\sin\alpha \sin\varphi \sin\theta + \cos\alpha \cos\theta]} d\ell' \quad (9b)$$

It is also clear from (5c) that the only contribution by the horizontal arm, to the Cartesian components of vector potential is

$$A_{yh} = \frac{\mu_0 e^{-j\beta_0 r}}{4\pi r} \int_b^{b+L_2} I(y') e^{j\beta_0 [y' \sin\varphi \sin\theta + L_1 \cos\alpha \cos\theta]} dy' \quad (9c)$$

According to the usual Cartesian-Spherical coordinates transformation identities given as

$$A_\theta = \cos\theta \cos\varphi A_x + \cos\theta \sin\varphi A_y - \sin\theta A_z \quad (10a)$$

and

$$A_\varphi = -\sin\varphi A_x + \cos\varphi A_y \quad (10b)$$

therefore, the spherical components of the vector potential emerge as

$$A_\theta = \frac{\mu_o e^{-j\beta_o r}}{4\pi r} \left( \int_0^{L_1} [\cos\theta \sin\phi \sin\alpha - \sin\theta \cos\alpha] I(\ell') e^{j\beta_o \ell' [\sin\alpha \sin\phi \sin\theta + \cos\alpha \cos\theta]} d\ell' + \cos\theta \sin\phi \int_b^{b+L_2} I(y') e^{j\beta_o [y' \sin\phi \sin\theta + L_1 \cos\alpha \cos\theta]} dy' \right) \quad (11a)$$

and

$$A_\phi = \frac{\mu_o e^{-j\beta_o r}}{4\pi r} \left( \int_0^{L_1} [\cos\phi \sin\alpha] I(\ell') e^{j\beta_o \ell' [\sin\alpha \sin\phi \sin\theta + \cos\alpha \cos\theta]} d\ell' + \int_b^{b+L_2} \cos\phi I(y') e^{j\beta_o [y' \sin\phi \sin\theta + L_1 \cos\alpha \cos\theta]} dy' \right) \quad (11b)$$

In the far-zone of the antenna, the radiated electric field components are, for the  $e^{j\omega t}$  harmonic time variation assumed and suppressed everywhere in this paper, are simply connected to the corresponding vector potential components according to

$$E_\theta = -j\omega A_\theta \quad \text{and} \quad E_\phi = -j\omega A_\phi \quad (12)$$

So that the desired electric field integral equations, in the case of the right arm are obtained as

$$E_\theta^R = \frac{-j\omega \mu_o e^{-j\beta_o r}}{4\pi r} \left( \int_0^{L_1} [\cos\theta \sin\phi \sin\alpha - \sin\theta \cos\alpha] I(\ell') e^{j\beta_o \ell' [\sin\alpha \sin\phi \sin\theta + \cos\alpha \cos\theta]} d\ell' + \int_b^{b+L_2} \cos\theta \sin\phi I(y') e^{j\beta_o [y' \sin\phi \sin\theta + L_1 \cos\alpha \cos\theta]} dy' \right) \quad (13a)$$

and

$$E_\phi^R = \frac{-j\omega \mu_o e^{-j\beta_o r}}{4\pi r} \left( \int_0^{L_1} [\cos\phi \sin\alpha] I(\ell') e^{j\beta_o \ell' [\sin\alpha \sin\phi \sin\theta + \cos\alpha \cos\theta]} d\ell' + \int_b^{b+L_2} \cos\phi I(y') e^{j\beta_o [y' \sin\phi \sin\theta + L_1 \cos\alpha \cos\theta]} dy' \right) \quad (13b)$$

In the antenna plane defined by  $\phi = 90^\circ$ , the phi-component of this field vanishes, and its theta-component reduces to

$$E_\theta^R = \frac{-j\omega \mu_o e^{-j\beta_o r}}{4\pi r} \left( \int_0^{L_1} [\sin(\alpha - \theta)] I(\ell') e^{j\beta_o \ell' \cos(\alpha - \theta)} d\ell' + \int_b^{b+L_2} \cos\theta I(y') e^{j\beta_o [y' \sin\theta + L_1 \cos\alpha \cos\theta]} dy' \right) \quad (14)$$

A case of particular interest here is that defined by  $\alpha = 0^\circ$ , for which the isolated right arm of the CVDA becomes a bent dipole antenna of the type referred to by [3, Fig. (10.11b)]. For this ‘bent wire’,

$$E_\theta^R = \frac{j\omega \mu_o e^{-j\beta_o r}}{4\pi r} \left( \int_0^{L_1} [\sin(\theta)] I(z') e^{j\beta_o z' \cos\theta} dz' - \int_0^{L_2} \cos\theta I(y') e^{j\beta_o [y' \sin\theta + L_1 \cos\theta]} dy' \right), \quad (15)$$

with  $E_\phi^R$  being zero, since  $b = L_1 \sin\alpha$ , is zero when  $\alpha = 0^\circ$ .

As earlier noted, the radiation zone field integral equations for the CVDA’s left arm derive from corresponding equations for the right arm through the replacement in the latter, of  $\alpha$  by  $-\alpha$  and  $y$  by  $-y$ . Accordingly therefore, it is easily verified that for the left arm,

$$E_\theta^L = \frac{j\omega \mu_o e^{-j\beta_o r}}{4\pi r} \left( \int_0^{L_1} [\cos\theta \sin\phi \sin\alpha + \sin\theta \cos\alpha] I(\ell') e^{j\beta_o \ell' [\cos\alpha \cos\theta - \sin\alpha \sin\phi \sin\theta]} d\ell' + \int_{-b}^{-(b+L_2)} \cos\theta \sin\phi I(-y') e^{j\beta_o [L_1 \cos\alpha \cos\theta - y' \sin\phi \sin\theta]} dy' \right) \quad (16a)$$

with

$$E_\phi^L = \frac{j\omega \mu_o e^{-j\beta_o r}}{4\pi r} \left( \int_0^{L_1} [\cos\phi \sin\alpha] I(\ell') e^{j\beta_o \ell' [\cos\alpha \cos\theta - \sin\alpha \sin\phi \sin\theta]} d\ell' + \int_{-b}^{-(b+L_2)} \cos\phi I(-y') e^{j\beta_o [L_1 \cos\alpha \cos\theta - y' \sin\phi \sin\theta]} dy' \right) \quad (16b)$$

A combination of (13) and (14) yields the total radiated field of the CVDA, for which the theta-component, for example, is given by

$$E_{\theta}^{cv} = \frac{-j\omega\mu_0 e^{-j\beta_0 r}}{4\pi r} \left[ \int_0^{L_1} [\cos\theta \sin\varphi \sin\alpha - \sin\theta \cos\alpha] I(\ell') e^{j\beta_0 \ell' [\sin\alpha \sin\varphi \sin\theta + \cos\alpha \cos\theta]} d\ell' + \int_b^{b+L_2} \cos\theta \sin\varphi I(y') e^{j\beta_0 [y' \sin\varphi \sin\theta + L_1 \cos\alpha \cos\theta]} dy' \right. \\ \left. - \int_0^{L_1} [\cos\theta \sin\varphi \sin\alpha + \sin\theta \cos\alpha] I(\ell') e^{j\beta_0 \ell' [\cos\alpha \cos\theta - \sin\alpha \sin\varphi \sin\theta]} d\ell' - \int_{-b}^{-(b+L_2)} \cos\theta \sin\varphi I(-y') e^{j\beta_0 [L_1 \cos\alpha \cos\theta - y' \sin\varphi \sin\theta]} dy' \right] \quad (17)$$

The only unknown quantity in integral equations for the radiation fields of the CVDA is the distribution of current on the antenna. And this is readily determined with the use of the Method of Moments [28] with piecewise linear (triangular) basis and weighting functions, in a manner prescribed, [29], for bent thin-wire structures. With the availability of the current distribution, it becomes a straightforward matter to evaluate the antenna's feed-point input impedance ( $Z_{in}$ ) as the ratio of excitation voltage ( $V_{in}$ ) to the feed-point current ( $I_{in}$ ), that is,

$$Z_{in} = \frac{V_{in}}{I_{in}} = R_{in} + jX_{in} \quad (18)$$

where  $R_{in}$  stands for input resistance and  $X_{in}$  input reactance, at the antenna's feed point. Other antenna performance-characterizing parameters evaluated include return loss for a  $50\Omega$  feed line, defined, [30], as

$$Return\ Loss(dB) = 20\log_{10} \left| \frac{Z_{in} + Z_o}{Z_{in} - Z_o} \right| \quad (19)$$

where  $Z_o = 50\Omega$ : as well as maximum directivity, using the standard formula:

$$D_{max}(dB) = 10\log_{10} \frac{P_{max}}{P_{ave}} \quad (20)$$

in which  $P_{max}$  represents maximum radiated power density and  $P_{ave}$  the average radiated power density.

### III. COMPUTATIONAL RESULTS AND DISCUSSION

#### A. Model Validation

For the purposes of validating the model developed through the formulation in section II, computational results due to the model are compared with two sets of results available from the literature [3], [27], and acquired with the use of commercial graph digitizer software, 'GETDATA'. The profiles of Fig. 2(a) and Fig. 2(b) compare computed input resistance and reactance, respectively, as available from [3, Chapter 10, section 10.2.1], and concerning a bent wire, which may be described as the right arm of a CVDA, for which the slant angle  $\alpha$  is set to zero.

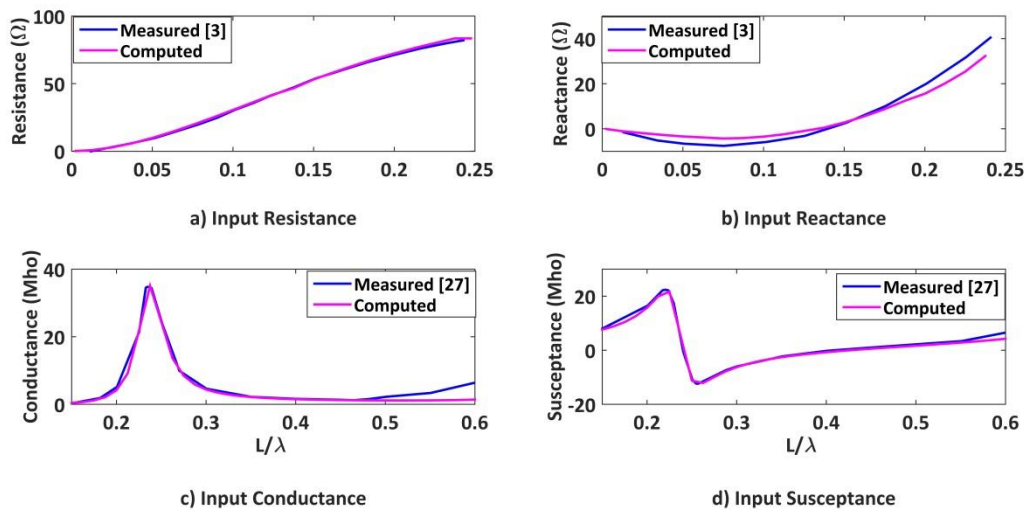


Fig. 2. Comparison of computational results with measurement data from [3] and [27].

On the other hand, the input admittance profiles of Fig. 2(c) and Fig. 2(d) are for the ‘Vee antenna’ referred to by [27, page 21], and modelled here as a compressed CVDA for which  $\gamma = 0$  and  $\alpha = 60^\circ$ . The very good agreements between the results due to the CVDA models and corresponding published data support the validity of this paper’s formulation.

### B. Current distribution

Representative profiles of the distribution of current along the arms of the CVDA (as defined by (2a) and (2b)) are displayed in Fig. 3(a), Fig. 3(b), Fig. 3(c), and Fig. 3(d); as well as Fig. 4(a), Fig. 4(b), Fig. 4(c), and Fig. 4(d), for different combinations of the antenna’s physical specifications. In both sets of figures, the horizontal (y-) axis (normalized to wavelength and identified as ‘ $y_\lambda$ ’) corresponds to the antenna arm axis in the manner described by Fig. 1(a). The profiles of Fig. 3(a), Fig. 3(b), Fig. 3(c), and Fig. 3(d), are, respectively, for slant angle values of  $30^\circ$ ,  $45^\circ$ ,  $60^\circ$  and  $75^\circ$ , when the antenna, operated at a frequency of 1.5GHz, has an arm length of  $0.25\lambda$ ; and those of Fig. 4(a), Fig. 4(b), Fig. 4(c), and Fig. 4(d), are also, respectively, for the same values of slant angle, but in this case, for  $L = 0.75\lambda$ . Computational results reported in this section derive from the MoM solution, in which a ‘delta-gap’ model of 1V has been utilized for the source.

It is readily observed from Fig. (3a) that when the slant angle ( $\alpha$ ) assumes a value of  $30^\circ$ , the magnitude of current distributes almost linearly on both arms of the antenna, extending from a maximum at the feed point, to zero at the tip of the horizontal segment.

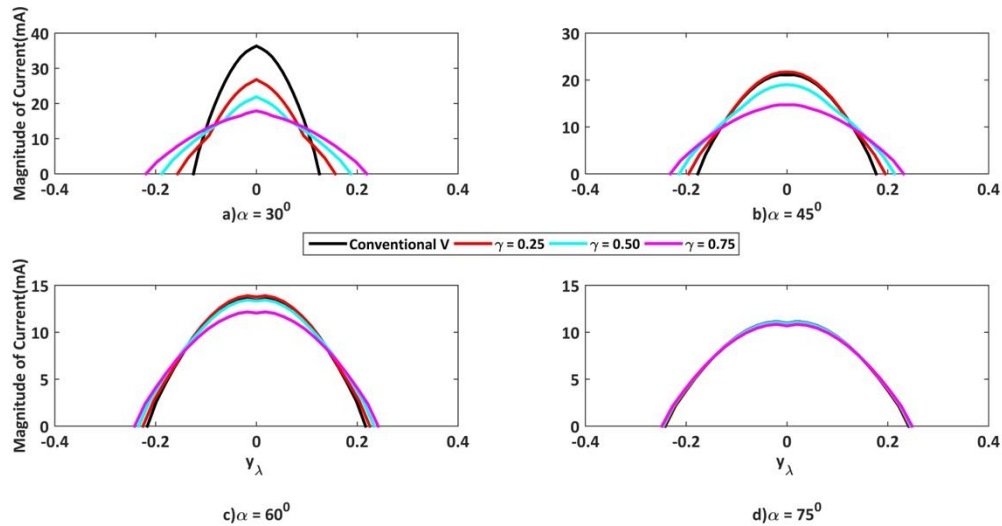


Fig. 3. Distribution of current on the axis of different configurations of the CVDA for  $L = \lambda/4$

Maximum value of magnitude of current decreases as  $\gamma$  increases from 0 (conventional V) to 0.75, when the CVDA geometry approaches that of a linear dipole. Fig. (3b) reveals that when the slant angle is increased to  $45^\circ$ , profiles of the magnitude of current now gently curves at the CVDA's apex, and maximum value of current magnitude for 0.25 compression now slightly exceeds that for the conventional vee. Profiles of current distribution displayed in Fig. (3c) and Fig. (3d) show that when the value of apex angle is such that the CDVA's geometry (for the value of L specified) approaches that of a half-wave dipole, current distributions for all degrees of compression, begin to converge to that characteristic of the dipole.

The current distribution profiles of Fig. 4(a), Fig. 4(b), Fig. 4(c), and Fig. 4(d) are those for the  $L = 3\lambda/4$  CVDA, but for the same values of compression and slant angle as in Fig. 3(a), Fig. 3(b), Fig. 3(c), and Fig. 3(d), respectively. These two sets of current distribution profiles share a number of features, including the facts that for any given  $\gamma$ , magnitude of current decreases as slant angle increases; and that the profiles converge as  $\alpha$  increases towards  $90^\circ$ .

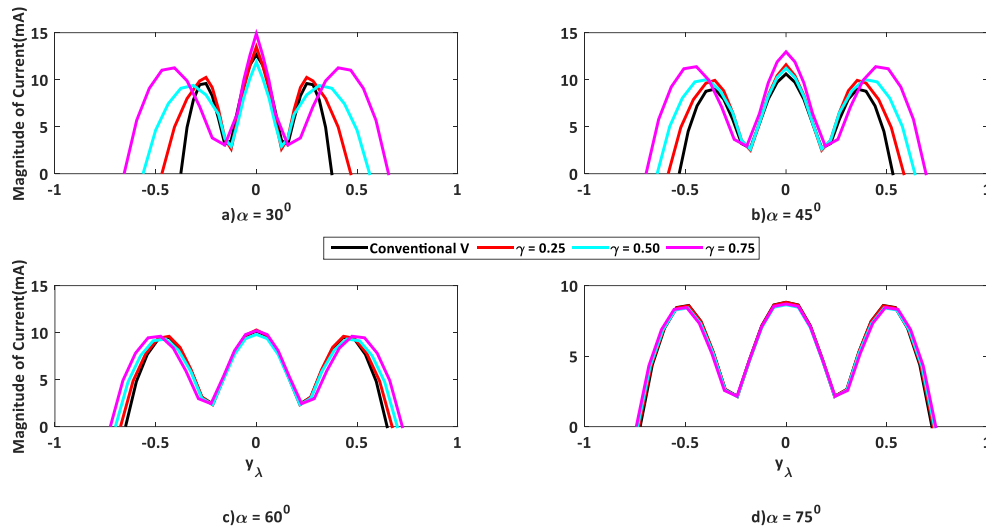


Fig. 4. Distribution of current on the axis of different configurations of the CVDA for  $L = \frac{3\lambda}{4}$

Unlike those of Fig. 3(a), Fig. 3(b), Fig. 3(c), and Fig. 3(d), however, the corresponding maximum value of magnitude of current is in the respective cases of Fig. 4(a), Fig. 4(b), Fig. 4(c), and Fig. 4(d), are generally associated with  $\gamma = 0.75$ , closely followed by  $\gamma = 0.25$ . In addition, a few cycles of variations have been introduced on account of the longer arm length.

### C. Input impedance, Return loss and Directivity

Characteristic features of the CVDA's input impedance, return loss, and maximum directivity, for the same parameters specified for the evaluation of current distribution, are respectively described by the curves of Fig. (5a), Fig. (5b), Fig. (5c), and Fig. (5d); as well as those of Fig. (6a), Fig. (6b), Fig. (6c), and Fig. (6d). From the profiles of Fig. (5a), Fig. (5b), Fig. (5c), and Fig. (5d) concerning the  $L = 0.25\lambda$  CDVA, it is readily seen that these parameters, in general, vary significantly with both slant angle and compression factor. For example, the value of input resistance recorded for  $\gamma = 0.75$  is generally higher than those for all other values of compression factor and follows a locus different from those of the others. This latter observation is also true of the return loss profiles of Fig. (5c), from which it can be seen that maximum values of  $R_{in}$  for all values of compression factor, except for  $\gamma = 0.75$ , occur when slant angle is about  $45^\circ$ , with  $\gamma = 0.5$  recording the highest, and the conventional V, the lowest values of  $R_{in}$ . The profiles of Fig. (5b) indicate that one important consequence of varying slant angle for the CVDA is to enable a shift in resonance, as compression factor changes.

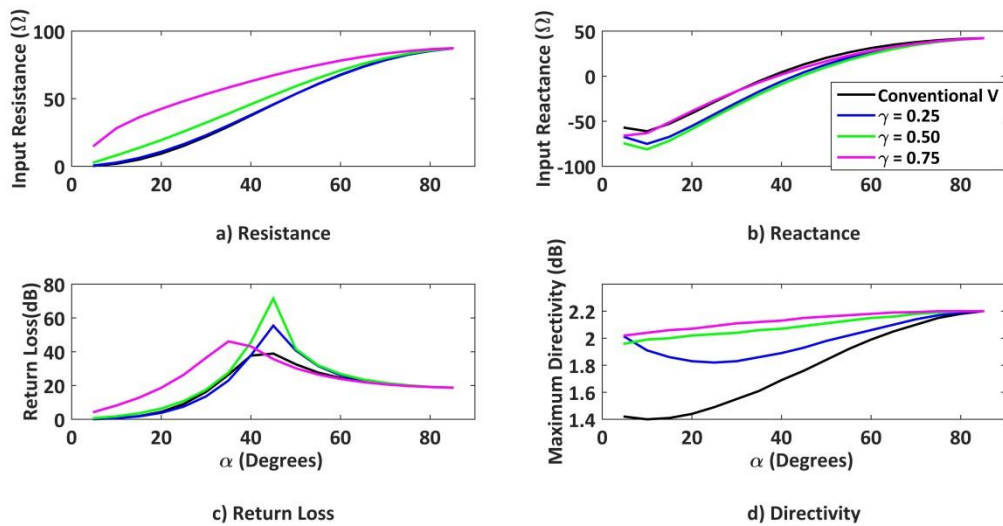


Fig. 5. Variations of input impedance, return loss, and maximum directivity of the  $L = 0.25\lambda$  CVDA with slant angle and degree of compression.

The directivity profiles of Fig. (5d) reveal that maximum CVDA directivity can be controlled through a choice of compression factor; but at the expense of some other parameters, as the profiles of the other parameters indicate. It is noteworthy to observe that all the profiles of Fig. (5a), Fig. (5b), Fig. (5c), and Fig. (5d) converge, as slant angle approaches  $75^\circ$ .

A radical departure in variations displayed in Fig. (5a), Fig. (5b), Fig. (5c), and Fig. (5d), for input impedance, return loss, and directivity, respectively, with changes in slant angle and compression factor, is recorded when CVDA's arm length becomes  $0.75\lambda$ . Notable differences, as can be seen from Fig. (6a), Fig. (6b), Fig. (6c), and Fig. (6d), include the facts that the locus of respective corresponding profiles now differ markedly, with input impedance and return loss values now demonstrating closer convergence at the slant angle of  $75^\circ$  than at  $50^\circ$ .

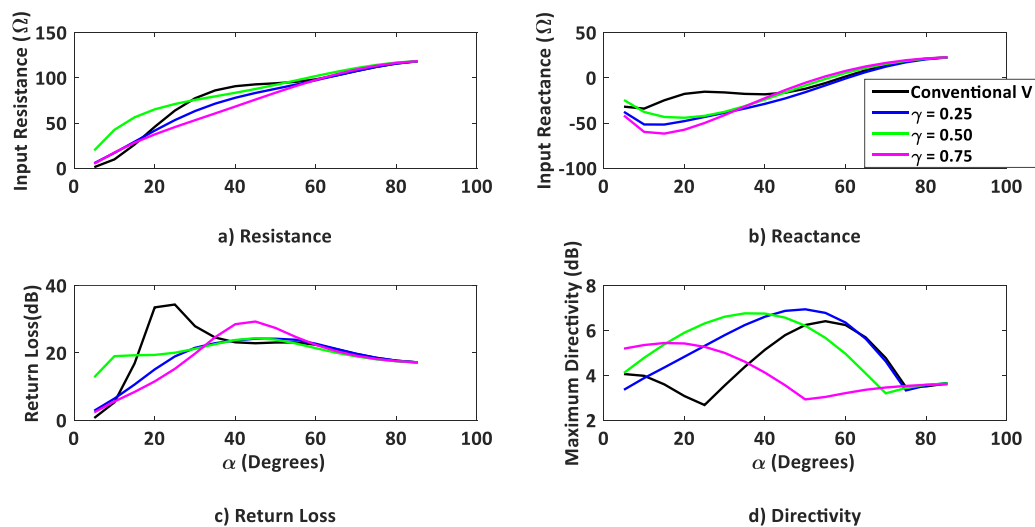


Fig. 6. Variations of input impedance, return loss, and maximum directivity of the  $L = 0.75\lambda$  CVDA with slant angle and degree of compression.

Maximum directivity for the compression factor of 0.75 is now recorded for a slant angle significantly smaller than those for the other compression factors, and the largest values are those for  $\gamma = 0.25$  and  $\gamma=0.5$ , in that order. An alternative perspective of how these performance parameters vary with CVDA arm's length is offered by the representative examples of Fig.(7a), Fig.(7b), Fig.(7c), Fig.(7d), and of Fig. (8a), Fig. (8b), Fig. (8c), and Fig. (8d). As a matter of fact, the curves of Fig. (7a) (for conductance) and Fig. (7c) (for return loss) explain the choices of  $L = 0.25\lambda$  and  $L = 0.75\lambda$  as arm length sizes in the preceding discussions. The return loss profiles of Fig. (7c) reveal that for a slant angle of  $30^\circ$ , maximum values of return loss are recorded when arm's length is a quarter wavelength, with the maxima for different values of compression factor decreasing in the decreasing order of  $\gamma$ . A set of 'local' return loss maxima are recorded when  $L = 0.75\lambda$ , generally significantly smaller than those at  $L = 0.25\lambda$ ; with the largest value being that for the conventional V, and all the other compression factors having about the same maximum values. In addition to occurring in no particular order of  $\gamma$ , maximum values of return loss in this case are distinctly larger than corresponding values recorded for the case  $\alpha = 30^\circ, L = 0.25\lambda$

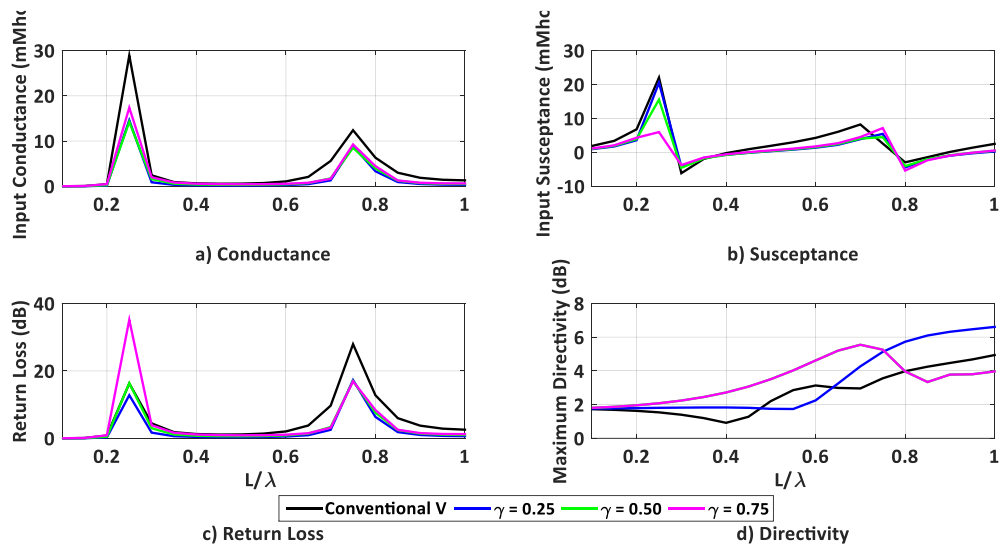


Fig. 7. Profiles of input admittance, return loss, and maximum directivity of the  $\alpha = 30^\circ$  CVDA with different compression factors.

As can be seen from the curves of Fig. (8a), Fig. (8b), Fig. (8c), and Fig. (8d), a scenario, essentially similar to that just described in the foregoing discussions, applies to the case of a  $45^\circ$  slant angle CVDA, though with a few notable differences.

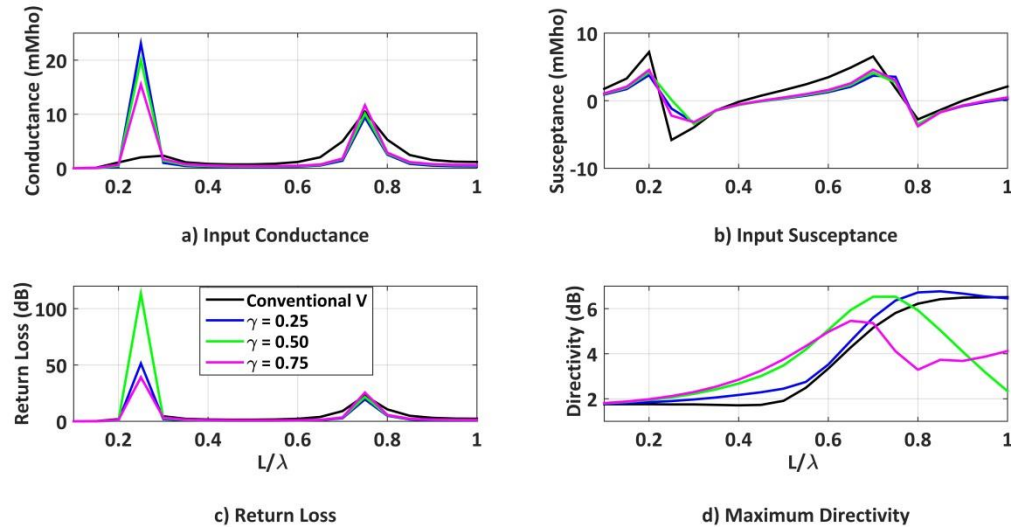


Fig. 8. Profiles of input admittance, return loss, and maximum directivity of the  $\alpha = 45^\circ$  CVDA with different compression factors.

It should also be mentioned that except for the maximum for  $\gamma = 0.5$  at  $L = 0.25\lambda$ , the sets of maxima for all values of  $\gamma$  at Fig. (3a),

#### D. Radiation-Zone Fields

The far-zone fields due to the current distributions of Fig. (3a), Fig. (3b), Fig. (3c), Fig. (3d), and Fig. (4a), Fig. (4b), Fig. (4c), and Fig. (4d), computed on the antenna plane  $\phi = 90^\circ$  with the use of (17) are displayed in Fig. (9a), Fig. (9b), Fig. (9c), Fig. (9d), and Fig. (10a), Fig. (10b), Fig. (10c), and Fig. (10d), for the set of respective cases associated with  $L = 0.25\lambda$  and  $L = 0.75\lambda$  CVDA. And for each set of cases, different compression factors and slants of the symmetric CVDA arms are specified. The  $E_\theta$  patterns of Fig. (9a) are for the cases of  $\alpha = 30^\circ$ , CVDA arm length of  $0.25\lambda$ , and compression factor ( $\gamma$ ) of 0, 0.25, 0.50 and 0.75: with  $\gamma = 0$  corresponding to the conventional V geometry. As may be expected, the patterns consist of two major lobes with virtually no sidelobes and maxima along the  $\theta = 0^\circ$  and  $\theta = 180^\circ$  axis. Nonetheless, the two-lobed patterns for  $\gamma = 0.5$  and  $0.75$  are more distinct than for other values of  $\gamma$ , with the case  $\gamma = 0$  having broadest major lobe beamwidth, thus highlighting one significance of compressing the arms of the conventional V-dipole. On the other hand, for  $\alpha = 45^\circ$ , the two-lobed patterns of Fig. (9b) are better formed for  $\gamma = 0.5$  and  $\gamma = 0.75$ , with some improvements over the two-lobed patterns when  $\gamma = 0$  and  $\gamma = 0.25$ , in comparison with the scenarios for the corresponding  $\alpha = 30^\circ$  cases

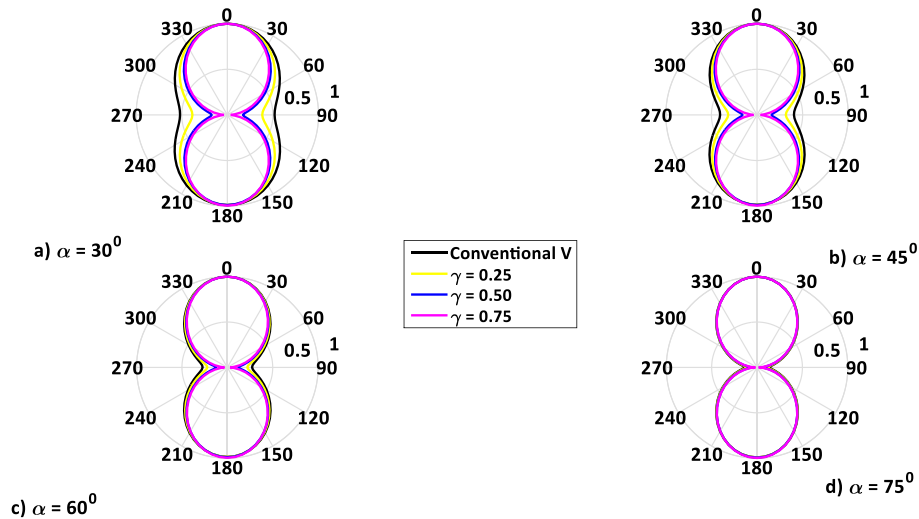


Fig. 9. Far-zone patterns for the  $L = 0.25\lambda$  CVDA corresponding to current distributions of Fig. 3.

Further improvements are observed when the slant angle  $\alpha$  is increased to  $60^\circ$  as evident in Fig. (9c) with moderate reduction in the major lobe beamwidths. And it is to be noted that for  $\alpha = 75^\circ$ , the two-lobed patterns for all degrees of compression are indistinguishable and entirely shaped without any minor lobes.

The set of field patterns displayed in Fig. (10a), Fig. (10b), Fig. (10c), and Fig. (10d), are for the  $L_\lambda = 0.75\lambda$  CVDA, for all values of  $\alpha$  and  $\gamma$  given consideration in this paper. Unlike the case of  $L_\lambda = 0.25\lambda$ , and consistent with the profiles of the current distributions of Fig. (4a), Fig. (4b), Fig. (4c), and Fig. (4d), the patterns in this case, are multi-lobed for all values of slant angle and compression factor specified here. It can be observed from Fig. (10a) ( $\alpha = 30^\circ$ ) for example, that the patterns have six lobes except for the case  $\gamma = 0$ , which has only four lobes even though not fully formed. Evidently, the maximum strengths of the fields, all occur along the  $\theta = 0^\circ$  axis, for practically all values of  $\gamma$ . When  $\alpha$  is increased to  $45^\circ$ , only the pattern for  $\gamma = 0.75$  retains the 6-lobed configuration, with the patterns of other cases of  $\gamma$  having several minor lobes; although the maxima for all the patterns are still featuring along the  $\theta = 0^\circ$  axis. Enhancements (more directive major lobes) in the 6-lobed pattern formation are observed when  $\alpha = 60^\circ$  with patterns corresponding to the case  $\gamma = 0.75$  being highly improved compared to other patterns.

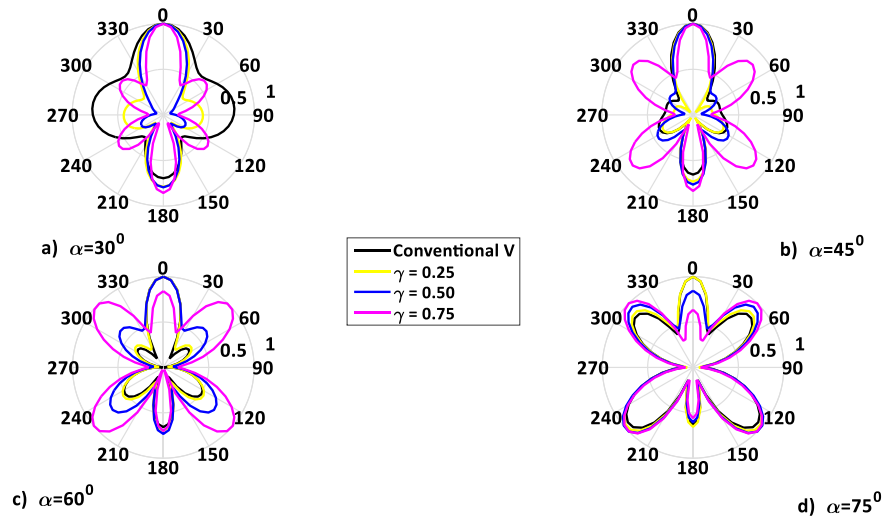


Fig. 10. Far-zone patterns for the  $L = 0.75\lambda$  CVDA corresponding to current distributions of Fig. 4.

It is worth noting that a virtually identical 6-lobed pattern was reported [31, Fig. 5-10] for the conventional V-dipole of  $0.75\lambda$  arm length and slant angle of  $59.25^\circ$ . This pattern according to [31] represents a significant improvement over that of the straight dipole, mainly on account of its reduced sidelobe level. Finally, when  $\alpha$  is set to a value of  $75^\circ$ , patterns, as seen from Fig. (10d), now converge in shape, and in the lower half of free space region, in size as well, in the upper half, along the  $\theta = 0^\circ$  axis.

It is particularly noteworthy that the patterns of Fig. (10a), Fig. (10b), Fig. (10c), and Fig. (10d) of this paper are remarkably similar to those of [26, Fig. (8)], which are reported to have been generated through simulations with the use of the commercial software, FEKO, and identified as being particularly suited to unmanned surface boat applications.

#### IV. CONCLUDING REMARKS

A theory has been developed in this paper, for the compressed V dipole antenna, recently introduced in the literature as being particularly suitable for unmanned surface boat applications. Following a comprehensive analytical description of the antenna's geometry, integral equations for its electric field intensity, in the far-zone was rigorously formulated. A method of moments solution to the integral equations provided an approximation to the distribution of current on the antenna, to enable a characterization of its performance parameters.

Computational results presented in the paper very clearly demonstrate how choice of arm length combines with slant (or apex) angle specification and 'compression factor', to determine the profiles of input impedance, return loss, directivity, and far-field patterns. The associated insights into the performance characteristics of the compressed V-dipole antenna reveal that the 'compression factor' is

an important design variable, through which any antenna performance parameter can be modified to suit specific application requirements.

With the availability of this theory, it is a fairly straight-forward matter to investigate the probable advantages of utilizing the CVDA (through resistive loading) for ground penetrating radar applications; unmanned surface boat applications, and satellite image acquisition applications.

## REFERENCES

- [1] G. Thiele and E. Ekelman, "Design formulas for vee dipoles", *IEEE Transactions on Antennas and Propagation*, vol. 28, no. 4, pp. 588-590, 1980. doi: 10.1109/TAP.1980.1142358.
- [2] D. M. Petković, and D. D. Krstić, "A new approach to v-dipole antenna", *FACTA UNIVERSITATIS Series: Working and Living Environmental Protection* vol. 2, no 2, pp. 143 – 149, 2002. <http://facta.junis.ni.ac.rs/walep/walep2002/walep2002-06.pdf>
- [3] C. A. Balanis, "Antenna Theory; Analysis and Design", John Wiley & Sons, Inc., New Jersey, pp. 543 – 547, 2016.
- [4] S. Licul, A. Safaai-Jazi and A. Chatzipetros, "Gain improvement and backlobe reduction in vee dipoles with director elements", *Proceedings of the IEEE Southeast Conference 2000. 'Preparing for The New Millennium'* (Cat. No.00CH37105), Nashville, TN, USA, pp. 182-188, 2000. doi: 10.1109/SECON.2000.845465.
- [5] N. Wells, "The quadrant aerial: an omni-directional wide-band horizontal aerial for short waves", *Journal of the Institution of Electrical Engineers - Part III: Communication Engineering*, vol. 91, pp. 182-193, 1944. doi: 10.1049/ji-3-1.1944.0040
- [6] R. King, "Theory of V Antennas", *Journal of Applied Physics*, vol. 22, pp. 1111-1121, 1951. doi: 10.1063/1.1700117
- [7] J. V. Surutka, D. M. Velikovi, "Input impedance of rectangular V - dipole antenna derived by variational method", *Publications de la Faculté d'électrotechnique de l'Université à Belgrade, Serie: Mathématique et Physique*, No 247 - 273, pp. 87 – 95. 1969. <https://www.jstor.org/stable/43667374>
- [8] J. H. Richmond. "Theoretical Study of V-antenna Characteristics for the ATS-E Radio Astronomy Experiments", *Scientific Report* 2619-1, Contract Number NAS5-11543, 2013. Electroscience Laboratory, Ohio State University. <https://apps.dtic.mil/sti/tr/pdf/AD0756470.pdf>
- [9] E. J. Jones, "Analysis of the symmetric center-fed V-dipole antenna", *IEEE Transactions on Antennas and Propagation*, vol. 24, no. 3, pp. 316-322, 1976. doi: 10.1109/TAP.1976.1141344.
- [10] B. Mangaraj, I. Misra, and A. Barisal, "Optimizing Included Angle of Symmetrical V-Dipoles for Higher Directivity Using Bacteria Foraging Optimization Algorithm", *Progress In Electromagnetics Research B*, vol. 3, 295-314, 2008 doi:10.2528/PIERB07121005
- [11] S. S. Sandler, "Radiation and Current Properties of the Resistively Loaded Traveling Wave V-antenna", *Scientific Report* No. 3, prepared for NASA under Grant N0, NsG 355 1966 . <https://ntrs.nasa.gov/api/citations/19660027935/downloads/19660027935.pdf>
- [12] S. S. Sandler, "Theory of the Resistively Loaded Traveling Wave V-antenna", *Scientific Report* No. 2, prepared for NASA under Grant N0, NsG 355, 1964. <https://ntrs.nasa.gov/api/citations/19650022573/downloads/19650022573.pdf>
- [13] K. Iizuka, "The traveling-wave v-antenna and related antennas", *IEEE Transactions on Antennas and Propagation*, vol. 15, no. 2, pp. 236-243, 1967. doi: 10.1109/TAP.1967.1138895.
- [14] K. Iizuka and R. W. P. King, "The Travelling Wave V Antenna", *Scientific Report* No. 5, Prepared for NASA under Grant No. NsG 579, 1965. <https://ntrs.nasa.gov/api/citations/19670006193/downloads/19670006193.pdf>
- [15] T. P. Montoya and G. S. Smith, "Resistively-loaded Vee antennas for short-pulse ground penetrating radar", *IEEE Antennas and Propagation Society International Symposium. 1996 Digest*, Baltimore, MD, USA, vol. 3, pp. 2068-2071 1996. doi: 10.1109/APS.1996.550015.
- [16] W. Kang and K. Kim, "Design and Fabrication of Resistively Loaded Dipoles using Planar Resistor Technology", 2018 *International Symposium on Antennas and Propagation (ISAP)*, Busan, Korea (South), pp. 1-2, 2018.
- [17] K. Kim and W. R. Scott, "Design of a resistively loaded vee dipole for ultrawide-band ground-penetrating Radar applications", *IEEE Transactions on Antennas and Propagation*, vol. 53, no. 8, pp. 2525-2532, 2005. doi: 10.1109/TAP.2005.852292.
- [18] N. Patwari and A. Safaai-Jazi, "High-gain low-sidelobe double-vee dipoles", *IEEE Transactions on Antennas and Propagation*, vol. 48, No. 2, pp. 333-335, 2000. doi: 10.1109/8.833086.
- [19] N. Patwari and A. Safaai-Jazi, "Predictions and measurements of double-vee dipoles", *IEEE Antennas and Propagation Society International Symposium. 1998 Digest. Antennas: Gateways to the Global Network. Held in conjunction with: USNC/URSI National Radio Science Meeting* (Cat. No.98CH36, Atlanta, GA, USA, vol. 3, pp. 1426-1429, 1998. doi: 10.1109/APS.1998.690774.
- [20] A. Mohamed and L. Shafai, "Investigation on vee dipole antennas for ultra-wideband applications", 2009 13th *International Symposium on Antenna Technology and Applied Electromagnetics and the Canadian Radio Science Meeting*, Banff, AB, Canada, PP. 1-4, 2009. doi: 10.1109/ANTEMURSI.2009.4805093.

- [21] M. Fathurahman, Zulhelman, A. Maulana, and M. Widyawati, "Design and Development of Dipole Antenna for NOAA Satellite Image Acquisition System and Processing," *Journal of physics; Conference Series* . 1364 012025, 2019. doi: 10.1088/1742-6596/1364/1/012025
- [22] S. Wagner and A.V. Pham, "The Ultrawideband Elliptical Resistively Loaded Vee Dipole", *IEEE Transactions on Antennas and Propagation*, vol. 68, no. 4, pp. 2523-2530, 2020. doi: 10.1109/TAP.2019.2949680.
- [23] J. Zhang, J. Yang and Q. Gong, "Electric field enhancing properties of the V-shaped optical resonant antennas", 2008 Conference on Lasers and Electro-Optics and 2008 Conference on Quantum Electronics and Laser Science, San Jose, CA, PP. 1-2, 2008. doi: 10.1109/CLEO.2008.4551986.
- [24] S. Lalithamma, N. P. Pathak, and S. K. Manhas, "Design and Analysis of Vee Dipole Based Reconfigurable Planar Antenna", *Progress in Electromagnetics Research Letters*, vol. 70, pp. 123-128, 2017. doi:10.2528/PIERL17080201
- [25] J. C. Mohsen, J. C., R. Pejman, and N. Kiani, "Reconfigurable graphene-based V-shaped dipole antenna: From quasi-isotropic to directional radiation pattern", *Optik*, vol. 184, pp. 421-427, 2019. <https://doi.org/10.1016/j.jjleo.2019.04.125>.
- [26] M. Xiu, L. Li, and S. Feng "Analysis of Radiation Characteristics of Compressed V-shaped Dipole Antenna", Unpublished Preprint Available from [https://assets.researchsquare.com/files/rs-1915248/v1\\_covered.pdf?c=1659552221](https://assets.researchsquare.com/files/rs-1915248/v1_covered.pdf?c=1659552221) 2022. doi: <https://doi.org/10.21203/rs.3.rs-1915248/v1>
- [27] D. Lekhyananda, "An Experimental Investigation of Modified Dipole Antennas", *Technical Report* 2648-1 The Ohio State University Electroscience Laboratory, 1969. <https://apps.dtic.mil/sti/tr/pdf/AD0692783.pdf>
- [28] R. F. Harrington, *Field computation by moment methods*, The Macmillan Book Company, New York, 1968.
- [29] D. C. Kuo, and B. J. Strait, "Improved programs for analysis of radiation and scattering by configuration of arbitrarily bent wires", *Syracuse University Scientific Report* No. 15, 1972. <http://ece-research.unm.edu/summa/notes/ln/0275.pdf>
- [30] T. S. Bird, "Definition and Misuse of Return Loss [Report of the Transactions Editor-in-Chief] ", *IEEE Antennas and Propagation Magazine*, vol. 51, no. 2, pp. 166-167, 2009. doi: 10.1109/MAP.2009.5162049.
- [31] W. L. Stutzman, and G. A. Thiele, *Antenna theory and design*, John Wiley & Sons, New York, pp. 204-205. 1981.